# Decomposition of Organochlorinated Silica Xerogels at High Temperature: A Kinetic Study

Beatriz Rosales-Reina , Guillermo Cruz-Quesada , Pablo Pujol , Santiago Reinoso , César Elosúa , Gurutze Arzamendi * , María Victoria López-Ramón , Julián J. Garrido *

Posted Date: 31 October 2025

doi: 10.20944/preprints202510.2450.v1

Keywords: hybris silica xerogels; adsorption; thermal stability; kinetic analysis; FWO method

 doi:10.20944/preprints202510.2450.v1



*Article*

# Decomposition of Organochlorinated Silica Xerogels at High Temperature: A Kinetic Study

**Beatriz Rosales-Reina [1], Guillermo Cruz-Quesada [2], Pablo Pujol [3], Santiago Reinoso [1], César Elosúa [4], Gurutze Arzamendi [1,*], María Victoria López-Ramón [2] and Julián J. Garrido [1,*]**

[1] Institute for Advanced Materials and Mathematics (INAMAT²), Departamento de Ciencias, Universidad Pública de Navarra (UPNA), Campus de Arrosadía, 31006 Pamplona, Spain

[2] Departamento de Química Inorgánica y Orgánica, Facultad de Ciencias Experimentales, Universidad de Jaén, 23071 Jaén, Spain

[3] Unidad Científico Técnica de Apoyo a la Investigación (UCTAI), Universidad Pública de Navarra (UPNA), Campus de Arrosadía, 31006 Pamplona, Spain

[4] Institute of Smart Cities (ISC), Departamento de Ingeniería Eléctrica, Electrónica y de Comunicación, Universidad Pública de Navarra (UPNA), Campus de Arrosadía, 31006 Pamplona, Spain

* Correspondence: garzamendi@unavarra.es (G.A.); j.garrido@unavarra.es (J.J.G.) Tel.: (+34 948 16 9601 (J.J.G))

**Abstract**

Hybrid silica xerogels functionalised with chlorinated organosilanes combine tunable porosity and surface chemistry, making them attractive for applications in sensing, membrane technology, and photonics. The main objective of this work is to investigate the thermal decomposition kinetics of organochlorinated xerogels and to establish a correlation with the released volatile compounds identified in a prior TGA/FTIR/GC–MS study. The materials were synthesised via the sol-gel process using organochlorinated alkoxysilane precursors and yielding highly condensed nanostructures in which the precursor nature strongly influences the morphology and textural properties. The $N_2$ adsorption analyses reveal that increasing the precursor content decreases the specific surface area and pore volume while promoting the formation of periodic domains, which are observed even at low organosilane molar percentages. The incorporation of such organic moieties imparts chemical reactivity and flexibility to the silica matrix, although it may also affect thermal stability, which is critical considering that decomposition can release hazardous volatiles such as benzene. A comprehensive thermal characterisation of a series of xerogels containing chloroalkyl and -aryl groups was conducted using TGA coupled to FT–IR and GC–MS, identifying two main decomposition stages and the following order of thermal stability according to the organosilane moiety: 4-chlorophenyl > chloromethyl > 3-chloropropyl > 2-chloroethyl. Kinetic and mechanistic insights were obtained through the Flynn–Wall–Ozawa isoconversional method and Criado master plots, using TGA/DSC measurements under nitrogen at multiple heating rates (5, 10, 20, 30 and 40 K $min^{-1}$). These results provide a framework for designing thermally stable hybrid materials for advanced technological applications.

**Keywords:** hybrid silica xerogel; adsorption; thermal stability; kinetic analysis; FWO method

## 1. Introduction

Within the field of organic-inorganic hybrid compounds, thermal stability defines the resistance of a material to elevated temperatures without undergoing degradation of its organic fractions and is a critical factor in maintaining both its structural integrity and functional performance in advanced applications [1,2]. Thermal decomposition can also involve the cleavage of inorganic bonds, which can compromise the overall structure and limit the technological applicability. In this context, hybrid xerogels have emerged as versatile materials, combining the chemical tunability of organic moieties with the robustness of an inorganic silica matrix. Their multifunctional nature enables a wide range

 doi:10.20944/preprints202510.2450.v1



of applications, including optical coatings [3,4], membranes [5,6], films [5,6], catalysts [9,10], as well as applications for biomedicine [11,12] and photonics [13–15]. Among these, hybrid xerogels functionalised with organochlorinated groups, the focus of this study, stand out due to their controlled microporosity and enhanced structural order [16–18], properties that could significantly expand their potential for novel technological applications.

These materials are synthesised through the sol–gel method, which introduces organic moieties either via silane coupling agents or through co-condensation reactions between functionalised silanes and tetraalkoxysilanes. This approach allows the incorporation of organic groups into the silica matrix in a single step, tailoring both the chemical and textural properties [19]. The presence of organic substituents also promotes the formation of locally ordered domains, mediated by weak interactions such as hydrogen bonding, dispersion forces, or π–π stacking [20].

Previous studies in our group [16–18] analysed the morphology, structure, and porous texture of four series of hybrid xerogels synthesised at pH 4.5 from ClRTEOS:TEOS blends with different molar percentages of organochlorinated ClRTEOS triethoxysilanes (ClR substituent = ClM, chloromethyl; ClE, 2-chloroethyl; ClP, 3-chloropropyl; ClPh, 4-chlorophenyl). Solid-state $^{29}$Si NMR spectroscopy confirmed the incorporation of organochlorinated substituents and the preservation of Si–C bonds. In the ClMTEOS and ClETEOS series, a high fraction of condensed $T^3$ species was detected, together with increasing proportions of $Q^3$ and $Q^4$ species as the ClRTEOS content rose. These findings indicate the formation of ordered structures, which is supported by the observation of low-angle X-ray diffraction signals indicating the contraction of Si–O–Si bonds relative to the non-chlorinated analogues. These organochlorinated series also displayed higher skeletal densities, attributable to steric and electronic effects of the functional groups. Field Emission SEM analyses revealed that increasing the ClRTEOS precursor concentration modified the material morphology from granular to smoother and more compact textures, accompanied by decreasing $N_2$ and $CO_2$ adsorption capacities, evidencing the tunability of the porous texture. Remarkably, cage-like $T_8$ periodic structures were detected even at low ClRTEOS precursor content (as in the material obtained from TEOS:ClETEOS blend with 99:1 molar ratio), reflecting profound structural and textural changes compared with reference non-chlorinated materials. Overall, chlorine substitution was shown to promote local structural order more effectively than using non-chlorinated analogous groups, expanding the prospects of the resulting materials for their use in membranes, catalysts, optical sensors, and optoelectronic devices.

A notable property of silica-based materials is their thermal stability, which determines the maximum temperature they can endure without decomposition. In a previous work [21], we analysed the vapours released during the thermal decomposition of hybrid xerogels with a 10% molar content of the ClRTEOS precursors listed above and detected several compounds posing environmental and health risks. Therefore, it is essential to characterise the thermal degradation kinetics to ensure both the material stability and environmental safety. Through TGA analysis, three mass loss stages were identified for these compounds: the first, common to all samples, corresponds to desolvation; the second, associated with the decomposition of the organochlorinated groups, varies depending on the precursor; and the third, also common to all samples, most likely involves the transformation of the hybrid xerogels into silicon oxycarbide ceramics [22]. In the second stage, simple decomposition mechanisms were identified for ClETEOS, whereas multiple mechanistic pathways were proposed for ClMTEOS, ClPTEOS, and ClPhTEOS based on the large collection of decomposition products detected. The established order of thermal stability was ClPhTEOS > ClMTEOS > ClPTEOS > ClETEOS, indicating the maximum temperature limits for safe use. The analysis of the vapours generated during pyrolysis was carried out by coupled to FT–IR and GC–MS tecnhiques, which enabled the precise identification and quantification of volatile products, as well as the determination of the temperatures at which they reach their maximum concentration.

The objective of this study is to investigate the thermal decomposition kinetics of the four organochlorinated xerogels mentioned above and to correlate the results with the most abundant substances identified in the prior TGA/FT–IR/GC–MS analyses [21]. This approach will help define a

 doi:10.20944/preprints202510.2450.v1



safe operational window for new applications. Thermal degradation of hybrid materials involves complex reaction mechanisms that can be elucidated through well-known mathematical models. In this context, model-free methods such as the Flynn–Wall–Ozawa (FWO) approach are particularly useful, as they do not require prior assumptions about the reaction mechanism. These methods enable the evaluation of the apparent activation energy, $E_\alpha$, which represents the energy barrier for characteristic stages of the global process. Additionally, the pre-exponential factor $A$, associated with the frequency of vibrations of the activated complex [23], can be deduced from $E_\alpha$. Finally, the molar enthalpy change ($\Delta H$) can also be deduced from $E_\alpha$, providing insight into the endothermic nature of the thermal decomposition process in siliceous materials.

Multiple stages are typically involved in the thermal decomposition of hybrid organic-inorganic materials [22], primarily focusing on desolvation and decomposition of the organic fraction. To identify an appropriate reaction model, $f(\alpha)$, the International Confederation of Thermal Analysis and Calorimetry (ICTAC) recommends the 'Z-master plot' method proposed by Criado for solid-state reactions [24]. According to the literature, the thermal degradation kinetics in inorganic materials typically conform to nucleation and growth models (An) [25]. In contrast, pyrolysis of organic matrices is best described by diffusion models (Dn) [26]. Meanwhile, n-order models (Fn) and geometrical contraction models (Rn) are applicable to all material types [27,28].

To the best of our knowledge, this study represents the first comprehensive analysis in which both kinetic and thermodynamic parameters of the thermal decomposition of hybrid silica xerogels are determined using FWO analysis and the Criado master plot methodology. These parameters are essential for assessing the thermal stability of organochlorinated-containing materials, predicting their performance in novel applications (e.g., sensor technologies), and mitigating potential emissions of toxic compounds in occupational environments.

## 2. Results and Discussion

Figure 1 schematises the methodologic procedure followed for the kinetic analysis of the thermal decomposition of organochlorinated silica xerogels in this work. This methodology consists of: 1) verifying that the $T$ vs conversion degree ($\alpha$) plots for different heating rates ($\beta$) do not intertwine, 2) applying the FWO method, 3) calculating the $E_\alpha$, and 4) determining the thermodynamic parameters ($\Delta H$ and $\Delta G$).

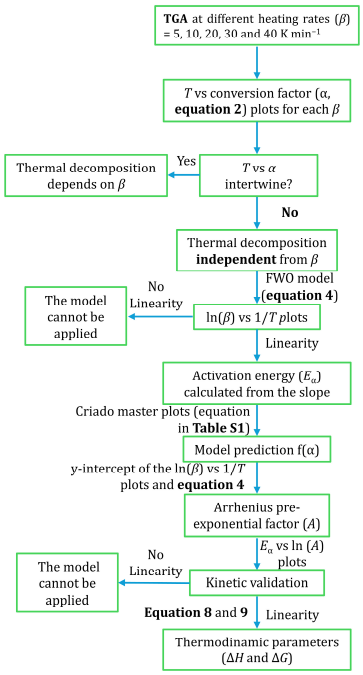

 doi:10.20944/preprints202510.2450.v1



**Figure 1.** Scheme of the procedure followed for the kinetic analysis of the thermal decomposition of organochlorinated hybrid silica xerogels.

*2.1. Thermal Analysis*

Figure 2 depicts the thermal evolution of the normalised mass loss ($m_{loss}$) of the reference xerogel (synthesised using only TEOS) and the four organochlorinated hybrid xerogels ClMTEOS, ClETEOS, ClPTEOS, and ClPhTEOS (with 10% molar content of the corresponding ClRTEOS precursor) for a heating rate ($\beta$) of 5 K min$^{-1}$. The evolutions for the rest of heating rates applied in the TGA analyses ($\beta$ = 10, 20, 30 and 40 K min$^{-1}$) are gathered in Figure S1. The different organic moieties of the ClRTEOS materials produced different behaviours during their decomposition at constant heating rates. Nevertheless, at least two distinct thermal decomposition stages are evident in all cases.

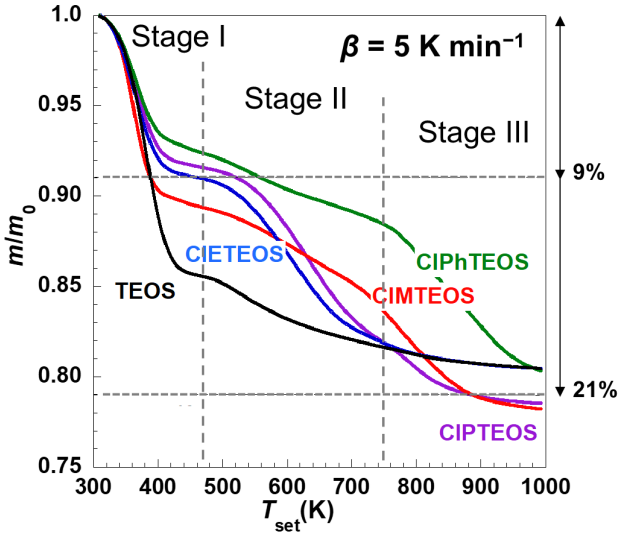


**Figure 2.** Evolution of the normalised mass as a function of the programmed temperature for the TEOS reference xerogel (black line) and the four organochlorinated ClRTEOS materials (lines: ClMTEOS, red; ClETEOS, blue; ClPTEOS, purple; and ClPhTEOS, green) at a heating rate of 5 K min$^{-1}$. The different degradation stages are marked with vertical grey lines.

While the total $m_{loss}$ during the overall process was approximately 20–22% in all cases, the relative mass fractions of the individual decomposition stages differed significantly between TEOS and ClRTEOS. Notably, the overall stability of TEOS is enhanced by the incorporation of just 10% of organochlorinated precursor. This enhancement can be attributed to a modified porous texture in the resulting xerogels, whereby the inclusion of such precursors reduces both the pore size distribution and the specific surface area, cancelling the mesoporous domain present in TEOS and diminishing the pore volume [21].

For the reference material, the first stage (desolvation) constitutes the primary decomposition process, whereas the principal $m_{loss}$ for the ClRTEOS materials occurs at higher temperatures (from 450-500 K up to 900-1000 K) and associates with the decomposition of organic fractions. The decomposition profiles of the hybrid xerogels prepared using 3-chloropropyl and 2-chloroethyl-containing triethoxysilane precursors (ClPTEOS and ClETEOS, respectively) are similar and display a steep $m_{loss}$ extending up to ca. 750 K as the second stage. These profiles differ from those of the materials prepared with the chloromethyl and 4-chlorophenyl derivatives (ClMTEOS and ClPhTEOS, respectively), which are alike and exhibit a progressive, extensive $m_{loss}$ that reaches higher temperatures between ca. 750 and 800 K instead.

According to literature kinetic analyses on the thermal decomposition of a methyl and vinyl-substituted polysiloxane, the temperatures at which the second stage takes place correspond to the

 doi:10.20944/preprints202510.2450.v1



release of volatile simple silane species such as $SiH_4$ and $CH_3SiH_3$, along with hydrogen and ethane, among others [22]. These molecules originate from the rearrangement of the bonding scheme involving the exchange of Si–O bonds with Si–H and/or Si–C bonds. In our previous investigations on the products released during the pyrolysis of organochlorinated xerogels [21], we could not identify any silanes, but mainly small molecules like $CO_2$ or HCl (accompanied with chloroethane) for ClMTEOS and ClETEOS, respectively, and larger species for ClPTEOS (cyclopropane, chloroethane) and ClPhTEOS (propene, chlorobenzene and a collection of chlorinated aromatics). The nature of the released vapours suggests that it is governed by dechlorination and chain-decomposition reaction mechanisms.

For all hybrid xerogels except ClETEOS, the thermal decomposition proceeds up to temperatures above 900 K with a further $m_{loss}$. In the case of organopolysiloxanes, this high-temperature third process (ca. 1000 K) has been attributed to various cleavage reactions of Si–H and Si–C bonds accompanied with the release of $CH_4$ and $H_2$ and the generation of free carbon clusters within the final silicon oxycarbide ceramic [22]. The formation of a silicon oxycarbide cannot be disregarded for organochlorinated silica xerogels, but the vapours released were identified to be mainly chloromethane for ClMTEOS, cyclopropane for ClPTEOS and chlorobenzene for ClPhTEOS [21]. In all cases, these molecules were accompanied by benzene and other heavier molecules, such as alkenes and dienes (hexadiene for ClMTEOS, butene and cyclopentadiene for ClPTEOS) or aromatic compounds (naphthalene for ClMTEOS, toluene for ClPTEOS and styrene for ClPhTEOS). These findings align with the fact that the formation of heavy organic compounds through chain cyclisation and aromatisation require higher decomposition temperatures. Thus, the decomposition behaviour of the hybrid xerogels differs markedly compared to the TEOS reference, which constitutes 90% of the composition in the ClRTEOS materials, indicating that the silica matrix is more thermally stable, whereas the chlorinated organosilane moieties are the most thermally susceptible.

The decomposition of the ClRTEOS materials at different heating rates faster than 5 K $min^{-1}$ ($\beta$ = 10, 20, 30 and 40 K $min^{-1}$) exhibit analogous decomposition profiles with the upper limits of the decomposition stages shifting toward higher temperatures as $\beta$ increases (Figure S1). The $m_{loss}$ in the initial desolvation stage decreases slightly with increasing the heating rate, except for TEOS and ClPhTEOS. Both materials undergo an increase in $m_{loss}$ within this stage, which is remarkable in the case of TEOS. Increasing $\beta$ causes thermal decomposition products to be released rapidly and the energy required for decomposition to be reached more quickly, as observed for these two xerogels (TEOS and ClPhTEOS). In the second stage, the $m_{loss}$ decreases slightly as the heating rate $\beta$ becomes faster in all materials except TEOS. In contrast, slight increases of $m_{loss}$ with $\beta$ are observed within the third stage, ClPhTEOS having the bigger $m_{loss}$.

Figure 3 shows the thermal evolution of both the first time-derivative of the normalised mass (DTG, top solid curves) and the normalised heat flux ($Q$, bottom dotted curves) of the TEOS reference and the four hybrid xerogels recorded at five different values of $\beta$. The DTG curves exhibit up to three minima, each one corresponding to each of the three decomposition stages. In the case of TEOS, the $m_{loss}$ above 750 K is negligible, thus the third stage cannot be confirmed from the $Q$ data. For ClPhTEOS and ClMTEOS, the second stage displays a notably flat profile (enclosed in a dashed box in Figure 3), which may compromise the accuracy of subsequent kinetic calculations.

In the $Q$ curves, the different endothermic signals are indicated on the graphs using arrows. For all the studied xerogels, the first two maxima are well defined and clearly distinguishable, while the third signal is in most cases not as clear because it is shadowed by that of the second stage and becomes difficult to be distinguished with enough definition. This third signal is best observed in the case of ClPTEOS, its maximum appearing centred at approximately 900 K. In all instances, the maxima corresponding to the second thermal stage display considerable width, suggesting that they likely encompass multiple overlapping processes of different nature.

 doi:10.20944/preprints202510.2450.v1



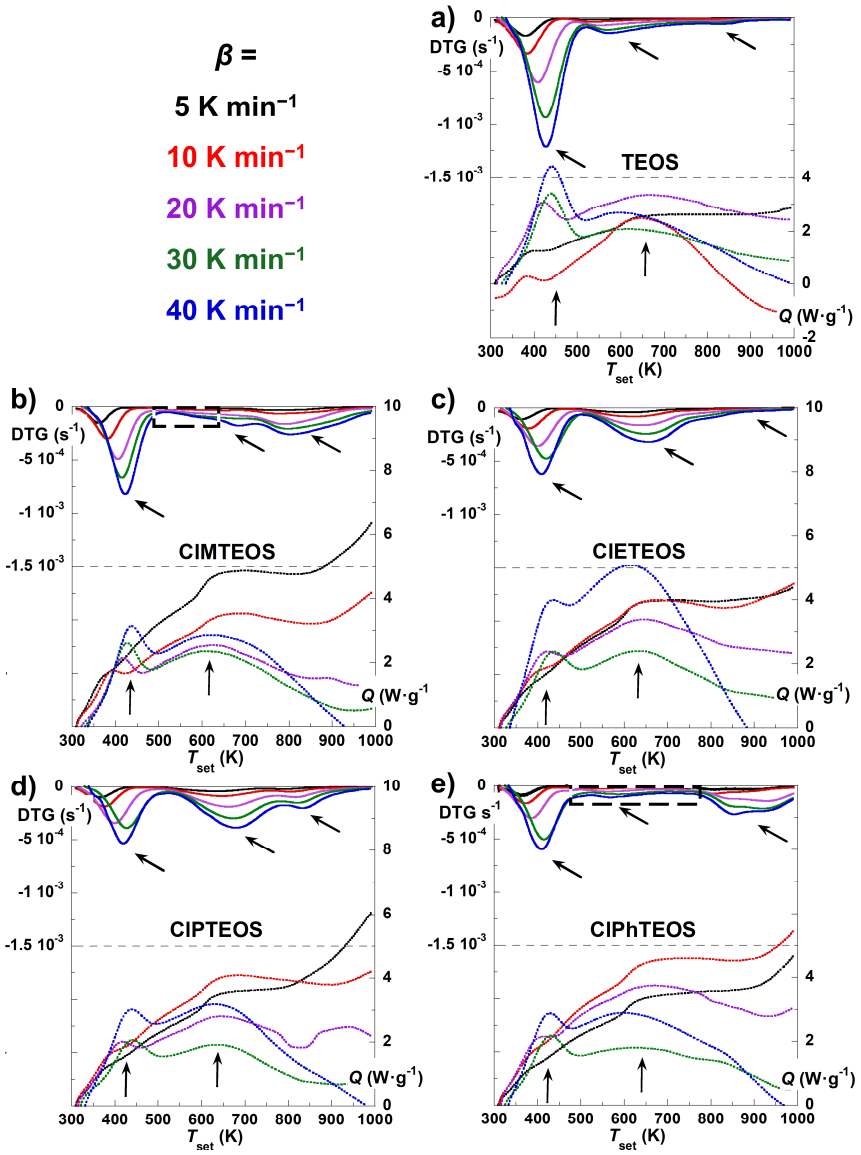


**Figure 3.** Evolution of the first-time derivative of the thermogravimetric curves (DTG, solid top curves) and the heat flow (*Q*, bottom dotted curves) as a function of the programmed temperature for the TEOS reference and the hybrid ClMTEOS, ClETEOS, ClPTEOS and ClPhTEOS xerogels.

### *2.2. Kinetic Analysis*

To perform a preliminary evaluation of the mechanism governing the global decomposition process, normalised Criado master plots were constructed for all xerogels after confirming that their T vs $\alpha$ plots for the five different heating rates do not intertwine significantly. The Criado master plots were obtained by following the methodology described in section 4.1 (see from equation 1 to 7) and the results are shown in Figure 4.

 doi:10.20944/preprints202510.2450.v1



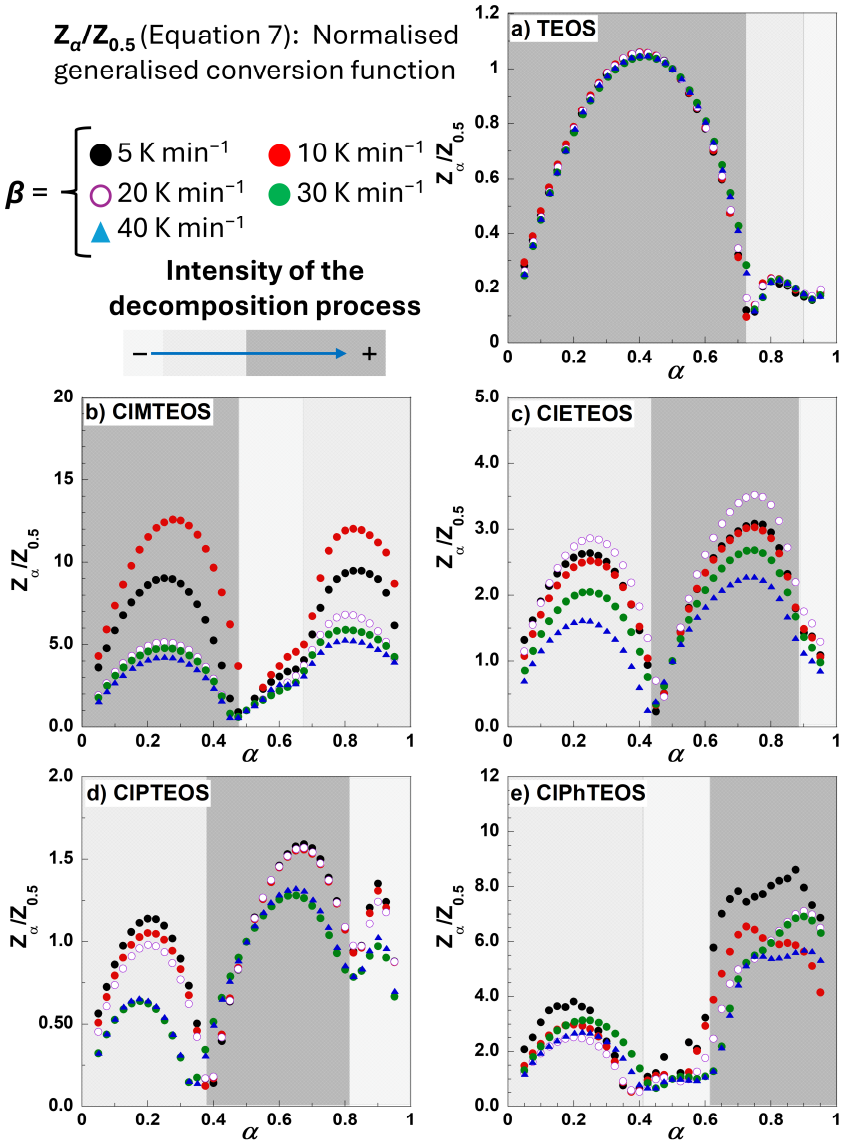


**Figure 4.** Criado master plots showing the evolution of the normalised generalised conversion function ($Z_\alpha/Z_{0.5}$) with the conversion degree $\alpha$ for the TEOS reference and the hybrid ClMTEOS, ClETEOS, ClPTEOS and ClPhTEOS xerogels.

The simplest behaviour is found in the case of TEOS, with the first stage serving as the principal governing process. For the organochlorinated xerogels, the first stage occurs at a conversion degree of approximately $\alpha$ = 0.4 (40% of the total $m_{loss}$), whereas the second and subsequent stages differ markedly in both the shape and extent of decomposition. The transition between the second and the third stages is not well defined, especially for ClMTEOS and ClPhTEOS, as the $Z_\alpha/Z_{0.5}$ curve does not reach a value of zero, indicating the initiation of an alternative mechanism. This transition is almost imperceptible for TEOS and ClETEOS.

To determine the kinetic decomposition mechanism using an isoconversional method, the first task was to identify the temperature intervals over which each stage develops and to define the fraction of mass lost in each case. For this work, this identification was guided by the shaded regions marked in Figure 4, determined by applying equation 4. According to the FWO method and by plotting ln($\beta$) against 1/$T$ within the $\alpha$ = 0.05–0.95 using increments of 0.025 [29], linear trends with regression coefficients higher than 0.97 were obtained for TEOS and ClPTEOS, as shown in Figure 5 (Figure S2 collects the ln($\beta$) vs 1/$T$ plots for the remaining three xerogel samples). The corresponding

 doi:10.20944/preprints202510.2450.v1



slopes are parallel, except within those temperature intervals where different mechanisms overlap, denoting the independence of the decomposition with $\beta$. This finding indicates a good agreement for the best fit to calculate the kinetic parameters.

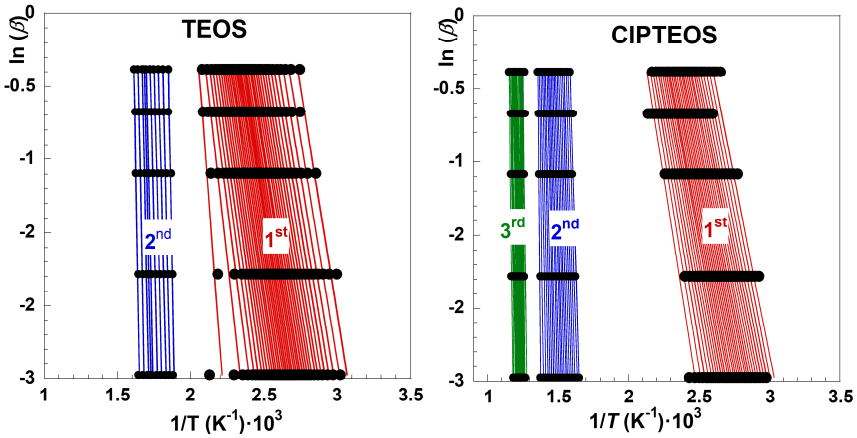


**Figure 5.** Linearity of the FWO method for the thermal decomposition of TEOS and ClPTEOS using ln($\beta$) vs 1/$T$ plots within the $\alpha$ = 0.05–0.95 range with increments of 0.025.

Although $\alpha$ varies from 0 to 1 in both graphs in Figure 5, the sensitivity of the study may not be equivalent within the whole range. The sensitivity will be linked to the relative mass loss of each stage, which is quite different for each xerogel sample studied in this work according to the results gathered in Figure 2. For example, the $m_{loss}$ associated with the first and second decomposition stages of TEOS corresponds to 14% and 6%, respectively, whereas $m_{loss}$ values of 8% and 12% are observed in the case of ClPTEOS, the third stage encompassing an additional $m_{loss}$ of 1%. The slope of the ln($\beta$) *vs* 1/$T$ lines increases as the stages evolve, and this trend was also found for rest of organochlorinated xerogels (Figure S2).

Figure 6 shows the variation of the activation energy ($E_\alpha$) with $\alpha$ obtained from the FWO method, where $E_\alpha$ exhibits different values for each decomposition stage, confirming the multi-step nature of the thermal decomposition [30]. The progressive increase in $E_\alpha$ with each subsequent stage indicates stable decomposition reactions and consistent disorder degree [31].

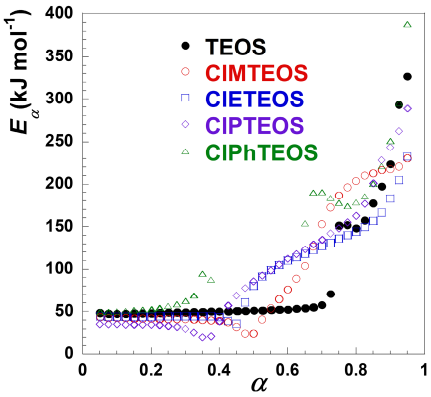


**Figure 6.** Variation of the activation energy with $\alpha$ obtained from the FWO method for the TEOS reference and the four ClRTEOS materials.

Table 1 summarises the minimum and the maximum values of $E_\alpha$ for each decomposition stage, which were calculated form the slope of the FWO plots using the methodologies described in section 4.1**.** The obtained values agree with the one found in the literature, considering that the errors are similar (in the 5–10% order), mainly due to the fitting of d$\alpha$/d$t$ [32].

 doi:10.20944/preprints202510.2450.v1



**Table 1.** Minimum and maximum values of the activation energy ($E_\alpha$) for each stage in the thermal decomposition of the TEOS reference and the four hybrid ClRTEOS materials.

| Xerogel | $E_\alpha$ (kJ mol$^{-1}$) | | |
|---|---|---|---|
| | **Stage I** | **Stage II** | **Stage III** |
| **TEOS** | 53 – 60 | 92 – 240 | – |
| **ClMTEOS** | 35 – 43 | – | 147 – 177 |
| **ClETEOS** | 47 – 53 | 93 – 158 | – |
| **ClPTEOS** | 41 – 42 | 74 – 186 | 205 – 252 |
| **ClPhTEOS** | 53 – 54 | – | 233 – 289 |

For the first stage, the $E_\alpha$ value ranges from 35 to 60 kJ mol$^{-1}$, which relates to the release of the surface physiadsorbed ethanol species. This process shows a direct correlation with the material textural properties, exhibiting higher $E_\alpha$ values for samples with wider mesoporous distribution [16–18]. The second stage covers the thermal decomposition of the chlorinated organosilane moieties and further condensation of the Si–OH groups. For this stage, the $E_\alpha$ values increase progressively with the thermal decomposition evolution, likely due to reduced accessibility of free silanol groups within the matrix. For the organochlorinated xerogels, the dehydroxylation reaction becomes less significant due to the lower amount of TEOS used in their preparation, resulting in silica matrices with lower abundance of Si–OH groups. However, the use of a 10% molar content of ClRTEOS precursors introduces additional, alternative decomposition pathways due to the organochlorinated moieties. Furthermore, the collapse of the matrix porosity reduces the diffusion rate of decomposition products [33]. Notably, the determination of $E_\alpha$ was precluded for ClMTEOS and ClPhTEOS due to the markedly flat DTG evolution in their second decomposition stages (marked with dashed boxes in Figure 3). Kappert et al. reported that the $E_\alpha$ values for the dehydroxylation reaction are highly dependent on the conversion degree, ca 150–300 kJ mol$^{-1}$, whereas the degradation of the functional group in organosilica matrices requires slightly lower values, 160–190 kJ mol$^{-1}$ [33].

Crucially, both the second and third decomposition stages (occurring above 420–500 K, depending on $\beta$) generate the most hazardous vapour species released from the thermal decomposition. Table 2 summarises the predominant species identified during the thermal decomposition of the ClRTEOS xerogels in a recent work [21], along with the characteristic temperature ranges for each mass loss stage. The first stages are associated with the diffusion process of ethanol out of the silica network. The second stages originate mainly from the dehydroxylation of the material, together with minor decomposition of the organic fragments from ClRTEOS moieties. The Si–C bonds break at the same time, bringing out the isolation of additional siloxane (Si–O–Si) bonds, which hinders the convergence of silanol groups and increases the dehydroxilation activation energy as a result. Hence, $E_\alpha$ increases with the conversion degree, and a higher value of energy is required for the thermal decomposition to proceed in agreement with the siloxane bonds stablished between the silanols. The third stage is only observed for ClMTEOS, ClPTEOS and ClPhTEOS and involves the highest $E_\alpha$ values, most likely because it relates to cyclisation and aromatisation of the organic fragments. Based on these results, ClPTEOS and TEOS demonstrated the highest thermal stability, while ClPhTEOS showed the lowest stability among the studied materials.

**Table 2.** Assignment of thermal decomposition and most abundant species in the studied xerogels.

| Xerogel | Stage | Predominant species* [21] | Temperature interval (5 K min$^{-1}$) | Process |
|---|---|---|---|---|
| TEOS | I | Ethanol | < 480 | Desolvation |
| | II | Ethanol | 480 – 780 | Dehydroxylation / Ethoxy group |
| ClMTEOS | I | Ethanol | < 470 | Desolvation |
| | II | [a] | 470 – 740 | Dehydroxylation / Ethoxy group |

 doi:10.20944/preprints202510.2450.v1



| | | | | |
|---|---|---|---|---|
| | III | **Chloromethane** / Naphthalene | >740 | Dechlorination / Aromatisation |
| ClETEOS | I | Ethanol | < 470 | Desolvation |
| | II | **Hydrochloric acid** / Chloroethane | 470 – 730 | Dehydroxylation / Ethoxy group/ Dechlorination |
| ClPTEOS | I | Ethanol | < 485 | Desolvation |
| | II | **Cyclopropane** / Chloroethane | 485 – 760 | Dehydroxylation / Ethoxy group/ Dechlorination |
| | III | **Cyclopropane** / Butene / toluene | > 760 | Dechlorination / Aromatisation |
| ClPhTEOS | I | Ethanol | <420 | Desolvation |
| | II | **Chlorobenzene** | 420-780 | Dehydroxylation / Ethoxy group/ Dechlorination |
| | III | **Chlorobenzene** / styrene | >780 | Dechlorination / Aromatisation |

* The most abundant species identified in the GC-MS are highlighted in bold. [a] The released species could not be unequivocally identified.

The values of $\Delta H$ calculated from equation 8 (Figure S3) were positive for all stages, reflecting the well-known, endothermic nature of the decomposition process. The numerical values were slightly lower (ca. 3–8 kJ mol$^{-1}$) than those of the corresponding $E_\alpha$. The values of $\Delta G$ were also calculated from equation 9 (Figure S4), resulting in positive high values as corresponds to non-spontaneous processes, which increase with the temperature required for the thermal decomposition.

The Criado master plot technique was employed to evaluate the most probable reaction model for all samples. Equation 7 was used to plot the theoretical and reduced rate curves of $Z_\alpha/Z_{0.5}$ against $\alpha$ for each decomposition stage of each sample using the mathematical expressions of the main kinetic models collected in Table S1. The best-fitting model was that of nth order kinetics, $F_n$. Figure 7 shows the experimental Criado master plots at $\beta$ = 5 K min$^{-1}$ for the TEOS reference and the four ClRTEOS materials compared to the predicted values for first, second and third order, $f(\alpha) = (1-\alpha)^n$, and for contracting geometrical models, being n = 1/2 for contracting area and n = 2/3 for contracting volume.

The comparison between the experimental and predicted Criado master plots for other considered models for solid-state reactions are included in Figure S5. All the hybrid xerogels display a similar experimental behaviour and the $F_n$ order models afforded the best fits. For the first stage, the experimental curve overlaps the F2 model when $\alpha$ is lower than 0.5, whereas at higher $\alpha$ values the experimental evolution lies between the first and second order. The behaviour for the second stage depends on the specific nature of the chlorinated organosilane moiety. While ClPTEOS follows the F1 model for almost the whole $\alpha$ range, the best fitting at $\alpha$ values lower than 0.5 corresponds to F2 for ClPhTEOS, the xerogels with the shorter alkyl chains (ClMTEOS and ClETEOS) deviating from the F3 model toward the F2 at low $\alpha$ values just above ca. 0.20. The trends above $\alpha$ = 0.5 are complex and do not adjust to any model except for ClMTEOS, which approaches the F1 model at high conversion degree. In the third stage, the analysis is more complex and the evolution for all the xerogels is included between the models F1 and F2, which could be due to the scarce $m_{loss}$ involved and the complex decomposition pathways resulting in silicon oxycarbide ceramics.

The selection of the best-fit reaction model was based on the calculation of the non-regression coefficient ($R^2$) and the lowest value of the root mean square error (RMSE). In the first stage the evolution is common for all matrices, with the second order being the one that fits the best. In the second and the third stages, the thermal degradation is more complex, as illustrated by the overlapping mechanisms in Figure 7. A reaction order greater than one is the result of the decrease in the decomposition rate with increasing $m_{loss}$. In heterogeneous reactions such as those in the present study, the reaction could be diffusion-controlled across an unstable interface that is reducing by a

 doi:10.20944/preprints202510.2450.v1



sintering process, or the accumulation of products at the interface could even lead to an increase of the diffusion resistance along the decomposition process.

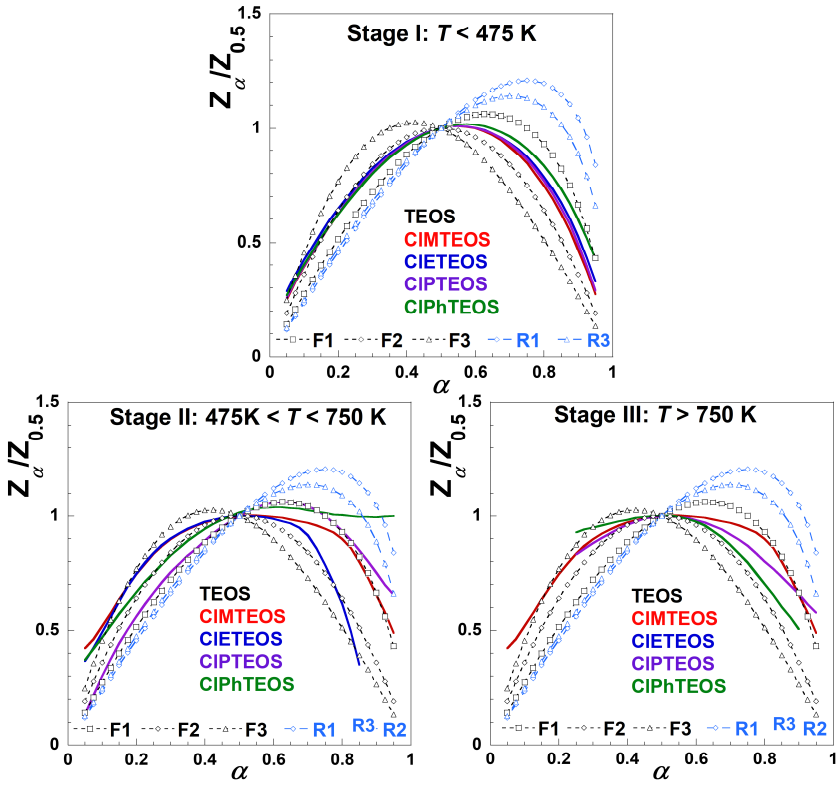


**Figure 7.** Criado master plots with the data from the isoconversional method (F1, F2, F3, R1 and R3 models in Table S1) for the TEOS reference and the hybrid xerogels ClMTEOS, ClETEOS ClPTEOS and ClPhTEOS.

## 3. Conclusions

This study evaluated the thermal decomposition kinetics of various organochlorinated silica xerogels. The results demonstrate a multi-step decomposition mechanism, with two to three distinct mass loss stages observed for both a pure silica reference (TEOS) and a series of hybrid silica materials with chloroalkyl and chlorophenyl groups. This work also confirms that characteristic species previously identified by GC–MS studies are generated and released at each decomposition stage. These stages were: (i) the release of physiadsorbed solvent, (ii) dehydroxylation and dechlorination of the material, and (iii) breaking of bonds between organic groups and silicon centres with consequent cyclisation and aromatisation. Nevertheless, this study found that much more complex mechanistic pathways are involved in each of these stages.

The nature of the organic moieties directly influences the studied thermal properties. The series of materials synthesised using chloroalkyltriethoxysilanes (chloromethyl, 2-chloroethyl and 3-chloropropyl) follow quite different thermal decomposition mechanisms, whereas that of the 4-chlorophenyl-containing xerogel closely resembles the one determined for the chloromethyl derivative. This is due to the reaction between alkyl chains radicals, which can favour the release of organic compounds or the collapse of the surface.

The FWO method provided results consistent with literature. The $E_\alpha$ increased with the evolution of the thermal degradation at each stage. The exponential nucleation, random nucleation and nuclei growth and diffusion models were not representative for the decomposition of the studied xerogels. Reaction order models afforded the best fitting, with the second and third order being the most suitable for all materials except ClPTEOS, which was best fitted to the first order due to the cyclisation capacity of the 3-chloropropyl moiety.

 doi:10.20944/preprints202510.2450.v1



These findings highlight the crucial importance of characterising the thermal stability of hybrid materials to ensure their safe and effective implementation in applications such as sensing devices. Since the temperature directly influences the sensor response characteristics, operating under thermal conditions above moderate temperatures can compromise the device performance. For the materials studied, a safe operational window below 450 K has been established to prevent thermal degradation and maintain the functionality.

## 4. Materials and Methods

Monoliths of the pure silica reference material (TEOS) and the four organochlorinated hybrid silica xerogels (ClMTEOS, ClETEOS, ClPTEOS, and ClPhTEOS) were obtained as described in previous works [16–18]. The xerogels were prepared through the sol–gel method in acidic conditions using blends of tetraethoxysilane (TEOS) and the corresponding ClRTEOS triethoxysilane (ClR substituent = ClM, chloromethyl; ClE, 2-chloroethyl; ClP, 3-chloropropyl; ClPh, 4-chlorophenyl) with a 90:10 molar ratio. A 10% content of organochlorinated groups is enough to the study of effect of the incorporation of such moieties into silica materials without compromising their structural integrity.

The monoliths were grounded and dried under vacuum for at least 12 h to extract their surface moisture before performing the thermogravimetric experiments (TGA/DTG), which were carried out under a $N_2$ flow of 40 mL $min^{-1}$ using a Mettler Toledo TGA/DSC 3+ series thermogravimetric analyser. Samples of approximately 15 mg were placed in 70 μL sapphire crucibles for thermal analysis from 303 to 1273 K at constant heating rates of 5, 10, 20, 30 and 40 K $min^{-1}$.

### *4.1. Methodology of Kinetic Studies*

For a single-step process, the reaction rate can be represented by the Equation (1):

$$\frac{d\alpha}{dt} = k\,(T) \cdot f(\alpha) = A_\alpha \cdot e^{-E_\alpha/R \cdot T} \cdot f(\alpha) \quad (1)$$

where $k(T)$ is the kinetic constant as a function of absolute temperature $T$; $f(\alpha)$ denotes the kinetic model function that depends on the reaction mechanism and the conversion degree $\alpha$; $A_\alpha$ is the Arrhenius pre-exponential factor, and $E_\alpha$ represents the apparent activation energy. The kinetic model is defined in terms of the global conversion $\alpha$, which represents the mass fraction volatilised. For each decomposition stage, $\alpha$ can be defined as follows:

$$\alpha_i = \frac{m_{o,i} - m_T}{m_{o,i} - m_{f,i}} \quad (2)$$

where $m_{o,i}$, $m_{T,i}$, and $m_{f,i}$ designate the initial, instantaneous, and final masses within each stage, respectively. Equation (3) displays the integral form of the kinetic model function, $g(\alpha)$:

$$g(\alpha) = \int_0^\alpha \frac{d\alpha}{f(\alpha)} = A_\alpha \cdot \int_0^\alpha e^{-E_\alpha/R \cdot T} \cdot dt \quad (3)$$

This integral does not have an exact analytical solution, but it can be solved by numerical approximation methods or by using other approximations proposed in the literature. For example, the Flynn-Wall-Ozawa (FWO) model [34] that employs the Doyle's approximation [35] can be applied for $20 \leq E_\alpha/R\ T \leq 60$ when the thermal decomposition is carried out a constant value of the heating rate $\beta$. At these conditions, Equation (3) can be rearranged as follows:

$$ln\beta = ln\left(\frac{A_\alpha \cdot E_\alpha}{R \cdot g(\alpha)}\right) - 5.331 - 1.052 \cdot \frac{E_\alpha}{R} \cdot \frac{1}{T_\alpha} \quad (4)$$

For isoconversional data, g($\alpha$), $A_\alpha$ and $E_\alpha$ have constant values. Thus, by registering the temperatures necessary ($T_\alpha$) to reach a particular decomposition degree $\alpha$ at different heating rates $\beta$, the activation energy $E_\alpha$ can be calculated from the slope of linear ln $\beta$ vs. $1/T_\alpha$ plots ($m = 1.052 \cdot E_\alpha/R$). The application of the isoconversional treatment allows to obtain $E_\alpha$ without considering any reaction model $f(\alpha)$.

 doi:10.20944/preprints202510.2450.v1



For thermal processes developed at a constant heating rate ($\beta$ =d$T$/d$t$), Equation (3) can be written as the following temperature integral having an analytical solution

$$g(\alpha) = \int_0^{\alpha} \frac{d\alpha}{f(\alpha)} = \frac{A_\alpha}{\beta} \cdot \int_0^{\alpha} e^{-E_\alpha/R \cdot T} \cdot dT = \frac{A_\alpha \cdot R \cdot T_\alpha{}^2}{E_\alpha \cdot \beta} \cdot \exp\left(\frac{-E_\alpha}{R \cdot T_\alpha}\right) \quad (5)$$

In this context, Criado proposed the use of the variable $Z(\alpha)$, which is defined as the product of differential and integral model contributions, $f(\alpha)\cdot g(\alpha)$, and the values of which can be easily calculated for each $\alpha$ from experimental TGA/DTG data [24]. The expression of $Z(\alpha)$ is given in Equation (6):

$$Z(\alpha) = f(\alpha) \cdot g(\alpha) = \frac{R \cdot T_\alpha{}^2}{E_\alpha \cdot \beta} \cdot \frac{d\alpha}{dt} \quad (6)$$

The mathematical expressions of $f(\alpha)$ and $g(\alpha)$ are well known for numerous kinetic models and Table S1 collects the equations for the main ones. Applying these expressions allows to calculate the theoretical values of $Z_\alpha$ for each $\alpha$. A Criado master plot consists of a representation against $\alpha$ of the values of the variable $Z(\alpha)$, either experimental or theoretical, normalised with the corresponding value at $\alpha$ = 0.5 according to Equation (7):

$$\left[\frac{Z(\alpha)}{Z(\alpha = 0.5)}\right]_{exp.} = \left(\frac{T_\alpha}{T_{\alpha=0.5}}\right)^2 \left[\frac{\left(d\alpha/dt\right)_\alpha}{\left(d\alpha/dt\right)_{\alpha=0.5}}\right] \quad (7)$$

The comparison of experimental and theoretical data by means of Criado master plots allows identifying the predominant kinetic mechanism within a thermal decomposition process, of organochlorinated hybrid silica xerogels in this case.

The implementation of the FWO method has important limitations, the first and main one being that the thermal decomposition cannot depend on $\beta$. Other limitations relate to the linear behaviour of the ln $\beta$ vs 1/$T$ or ln $\beta$ vs ln $A$ plots. Figure 1 schematises the calculation procedure followed in this work for implementing and validating the FWO method. Once the validation is satisfactorily completed, the molar enthalpy ($\Delta H$) and Gibbs energy ($\Delta G$) changes can be calculated through Equations (8) and (9) [36,37]:

$$\Delta H = E_\alpha - R \cdot T_m \quad (8)$$

$$\Delta G = E_\alpha + R \cdot T_m \cdot \ln\left(\frac{K_B \cdot T_m}{h \cdot A}\right) \quad (9)$$

where $T_m$ is the maximum decomposition temperature, $K_B$ is Boltzmann constant ($1.381 \cdot 10^{-23}$ J K$^{-1}$) and $h$ is Planck constant ($6.626 \cdot 10^{-34}$ J s).

**Supplementary Materials:** The following supporting information can be downloaded at: Preprints.org, Figure S1: Evolution of the normalised mass as a function of the programmed temperature for the TEOS reference and the four organochlorinated ClRTEOS materials at heating rates of 10, 20, 30 and 40 K min$^{-1}$; Figure S2: Linearity of the FWO method for the thermal decomposition of ClMTEOS, ClETEOS and ClPhTEOS using ln($\beta$) vs 1/$T$ plots within the $\alpha$ = 0.05–0.95 range with increments of 0.025; Figure S3: Dependence of the molar enthalpy change with $\alpha$ for the TEOS reference and the four organochlorinated ClRTEOS xerogels; Figure S4: Dependence of the Gibbs energy change with $\alpha$ for the TEOS reference and the four organochlorinated ClRTEOS xerogels; Figure S5: Criado master plots for the three decomposition stages of the TEOS reference and the four organochlorinated ClRTEOS materials using the different $P_n$, $A_n$, $D_n$, and $R_n$ models collected in Table S1; Table S1: Fitting performance of various kinetic models with different values of $f(\alpha)$ and $g(\alpha)$.

**Author Contributions:** B.R.-R.: investigation, data curation and writing—original draft. G.C.-Q.: formal analysis, writing—review and editing. P.P.: investigation. S.R.: funding acquisition, writing—review and editing.; C.E.: writing—review and editing.; G.A.: data curation, writing—review and editing.; M.V.L.-R.:

 doi:10.20944/preprints202510.2450.v1



writing—review and editing; J.J.G.: conceptualization, funding acquisition, project administration, supervision, writing—review and editing. All authors have read and agreed to the published version of the manuscript.

**Funding:** This work was supported by the projects PID2020-113558RB-C42, PID2022-137437OB-I00 and PID2022-142169OB-I00, funded by MCIN/AEI/10.13039/501100011033.

**Institutional Review Board Statement:** Not applicable.

**Informed Consent Statement:** Not applicable.

**Data Availability Statement:** The data presented in this study are available on request from the corresponding author.

**Acknowledgments:** J.J.G. and S.R., C.E. and M.V.L.-R. acknowledge the financial support from Ministerio de Ciencia e Innovación, Government of Spain and the Spanish Agencia Estatal de Investigación (projects PID2020-113558RB-C42, PID2022-137437OB-I00 and PID2022-142169OB-I00, respectively). The authors thank the technical and human resources from UCTAI (UPNA).

**Conflicts of Interest:** The authors declare no conflict of interest.

## Abbreviations

The following abbreviations are used in this manuscript:

| | |
|---|---|
| TEOS | Tetraethoxysilane |
| ClMTEOS | (Chloromethyl)triethoxysilane |
| ClETEOS | (2-Chloroethyl)triethoxysilane |
| ClPTEOS | (3-Chloropropyl)triethoxysilane |
| ClPhTEOS | (2-Chlorophenyl)triethoxysilane |
| FWO | Flynn–Wall–Ozawa |
| $E_\alpha$ | Activation energy |
| $\Delta H$ | Variation of the molar enthalpy |
| ICTAC | International Confederation of Thermal Analysis and Calorimetry |
| An | Nucleation and growth models |
| Dn | Diffusion models |
| Fn | n-Order models |
| Rn | Geometrical contraction |
| $\alpha$ | Conversion factor |
| $\beta$ | Heating rate |
| $m_{loss}$ | Mass loss |
| $Q$ | Heat flux |
| $Z_\alpha/Z_{0.5}$ | Normalised generalised conversion function |

## References

1. Ochoa, M.; Durães, L.; Matos Beja, A.; Portugal, A. Study of the suitability of silica based xerogels synthesized using ethyltrimethoxysilane and/or methyltrimethoxysilane precursors for aerospace applications. *J. Sol-Gel Sci. Technol*. **2012**, *61*, 151–160, doi: 10.1007/s10971-011-2604-7.
2. Pottathara, Y.B.; Bobnar, V.; Finšgar, M.; Grohens, Y.; Thomas, S.; Kokol, V. Cellulose nanofibrils-reduced graphene oxide xerogels and cryogels for dielectric and electrochemical storage applications. *Polymer* **2018**, *147*, 260–270, doi: 10.1016/j.polymer.2018.06.005.
3. Lee, S.; Gwon, K.; Kim, H.; Park, B.J.; Shin, J.H. High-performance amperometric carbon monoxide sensor based on a xerogel-modified PtCr/C microelectrode. *Sens. Actuators, B* **2022**, *369*, 132275, doi: 10.1016/j.snb.2022.132275.
4. Myadam, N.L.; Nadargi, D.Y.; Gurav Nadargi, J.D.; Shaikh, F.I.; Suryavanshi, S.S.; Chaskar, M.G. A facile approach of developing Al/$SnO_2$ xerogels via epoxide assisted gelation: A highly versatile route for formaldehyde gas sensors. *Inorg. Chem. Commun*. **2020**, *116*, 107901, doi: 10.1016/j.inoche.2020.107901.

 doi:10.20944/preprints202510.2450.v1




5. Rahman, S.K.; Maimunawaro; Rahma, A.; Syauqiah, I.; Elma, M. Functionalization of hybrid organosilica based membranes for water desalination – Preparation using Ethyl Silicate 40 and P123. *Mater. Today Proc*. **2020**, *31*, 60–64, doi: 10.1016/j.matpr.2020.01.187.
6. Xu, M.; Wang, X.; Zhou, B.; Zhou, L. Pre-coagulation with cationic flocculant-composited titanium xerogel coagulant for alleviating subsequent ultrafiltration membrane fouling by algae-related pollutants. *J. Hazard. Mater*. **2021**, *407*, 124838, doi: 10.1016/j.jhazmat.2020.124838.
7. Souto, F.T.; Machado, V.G. Hybrid films composed of ethyl(hydroxyethyl)cellulose and silica xerogel functionalized with a fluorogenic chemosensor for the detection of mercury in water. *Carbohydr. Polym*. **2023**, *304*, 120480, doi: 10.1016/j.carbpol.2022.120480.
8. Yao, H.; Kan, X.-T.; Zhou, Q.; Niu, Y.-B.; Zhang, Y.-M.; Wei, T.-B.; Lin, Q. Lanthanide-mediated cyclodextrin-based supramolecular assembly-induced emission xerogel films: A transparent multicolor photoluminescent material. *ACS Sustainable Chem. Eng*. **2020**, *8*, 13048–13055, doi: 10.1021/acssuschemeng.0c04490.
9. Styskalik, A.; Kordoghli, I.; Poleunis, C.; Delcorte, A.; Aprile, C.; Fusaro, L.; Debecker, D.P. Highly porous hybrid metallosilicate materials prepared by non-hydrolytic sol-gel: Hydrothermal stability and catalytic properties in ethanol dehydration. *Microporous Mesoporous Mater.* **2020**, *297*, 110028, doi: 10.1016/j.micromeso.2020.110028.
10. Styskalik, A.; Kordoghli, I.; Poleunis, C.; Delcorte, A.; Moravec, Z.; Simonikova, L.; Kanicky, V.; Aprile, C.; Fusaro, L.; Debecker, D.P. Hybrid mesoporous aluminosilicate catalysts obtained by non-hydrolytic sol–gel for ethanol dehydration. *J. Mater. Chem. A* **2020**, *8*, 23526–23542, doi: 10.1039/D0TA07016E.
11. Zhou, H.-J.; Teng, S.-H.; Zhou, Y.-B.; Qian, H.-S. Green strategy to develop novel drug-containing poly (ε-caprolactone)-chitosan-silica xerogel hybrid fibers for biomedical applications. *J. Nanomater*. **2020**, *2020*, 6659287, doi: 10.1155/2020/6659287.
12. Wendels, S.; de Souza Porto, D.; Avérous, L. Synthesis of biobased and hybrid polyurethane xerogels from bacterial polyester for potential biomedical applications. *Polymers* **2021**, *13*, 4256, doi: 10.3390/polym13234256.
13. Cruz, M.E.; Durán, A.; Balda, R.; Fernández, J.; Mather, G.C.; Castro, Y. A new sol-gel route towards $Nd^{3+}$-doped $SiO_2$-$LaF_3$ glass-ceramics for photonic applications. *Mater. Adv.* **2020**, *1*, 3589–3596, doi: 10.1039/d0ma00708k.
14. Vilela, R.R.C.; Zanoni, K.P.S.; de Oliverira, M., Jr.; de Vicente, F.S.; de Camargo, A.S.S. Structural and photophysical characterization of highly luminescent organosilicate xerogel doped with Ir(III) complex. *J. Sol-Gel Sci. Technol.* **2022**, *102*, 236–248, doi: 10.1007/s10971-021-05593-z.
15. Rosales-Reina, B.; López-Torres, D.; Cruz-Quesada, G.; Espinal-Viguri, M.; Elosúa, C.; Reinoso, S.; Garrido, J.J. Tuning the sensitivity of photonic sensors toward alkanes through the textural properties of hybrid xerogel coatings. *Adv. Funct. Mater.* **2025**, *35*, 2413871, doi: 10.1002/adfm.202413871.
16. Cruz-Quesada, G.; Espinal-Viguri, M.; López-Ramón, M.V.; Garrido, J.J. Novel organochlorinated xerogels: From microporous materials to ordered domains. *Polymers* **2021**, *13*, 1415, doi: 10.3390/polym13091415.
17. Cruz-Quesada, G.; Espinal-Viguri, M.; López-Ramón, M.V.; Garrido, J.J. Hybrid xerogels: Study of the sol-gel process and local structure by vibrational spectroscopy. *Polymers* **2021**, *13*, 2082, doi: 10.3390/polym13132082.
18. Cruz-Quesada, G.; Espinal-Viguri, M.; López-Ramón, M.V.; Garrido, J.J. Novel silica hybrid xerogels prepared by co-condensation of TEOS and ClPhTEOS: A chemical and morphological study. *Gels* **2022**, *8*, 677, doi: 10.3390/gels8100677.
19. Sanchez, C.; Soler-Illia, G. J. de A. A.; Ribot, F.; Lalot, T.; Mayer, C.R.; Cabuil, C. Designed hybrid organic-inorganic nanocomposites from functional nanobuilding blocks. 2001, *Chem. Mater*. **2001**, *13*, 10, 3061–3083, doi: 10.1021/cm011061e.
20. D'Angelo, A.; Mortalò, C.; Comune, L; Raffani, G.; Fiorentino, M.; Catauro, M. Sol–gel synthesized silica/sodium alginate hybrids: Comprehensive physico-chemical and biological characterization. *Molecules* **2025**, *30*, 3481, doi: 10.3390/molecules30173481.

 doi:10.20944/preprints202510.2450.v1




21. Rosales-Reina, B.; Cruz-Quesada, G.; Pujol, P.; Reinoso, S.; Elosúa, C.; Arzamendi, G.; López-Ramón, M.V.; Garrido, J.J. Determination of hazardous vapors from the thermal decomposition of organochlorinated silica xerogels with adsorptive properties. *Environ. Res.* **2024**, *256*, 119247, doi: 10.1016/j.envres.2024.119247.
22. García-Garrido, C.; Sánchez-Jiménez, P.E.; Pérez-Maqueda, L.A.; Perejón, A.; Criado, J.M. Combined TGA-MS kinetic analysis of multistep processes. Thermal decomposition and ceramification of polysilazane and polysiloxane preceramic polymers. *Phys. Chem. Chem. Phys*. **2016**, *18*, 29348–29360, doi: 10.1039/c6cp03677e.
23. Mortezaeikia, V.; Tavakoli, O.; Khodaparasti, M.S. A review on kinetic study approach for pyrolysis of plastic wastes using thermogravimetric analysis. *J. Anal. Appl. Pyrolysis* **2021**, *160*, 105340, doi: 10.1016/j.jaap.2021.105340.
24. Criado, J.M. Kinetic analysis of DTG data from master curves. *Thermochim. Acta* **1978**, *24*, 186–189, doi: 10.1016/0040-6031(78)85151-X.
25. Yang, J.; Liang, Q.; Hou, H. Thermal decomposition mechanism and kinetics of Pd/$SiO_2$ nanocomposites in air atmosphere. *J. Therm. Anal. Calorim*. **2019**, *135*, 2733–2745, doi: 10.1007/s10973-018-7673-1.
26. Açikalin, K. Determination of kinetic triplet, thermal degradation behaviour and thermodynamic properties for pyrolysis of a lignocellulosic biomass. *Bioresour. Technol*. **2021**, *337*, 125438, doi: 10.1016/j.biortech.2021.125438.
27. Sánchez-Jiménez, P.E.; Pérez-Maqueda, L.A.; Perejón, A.; Criado, J.M. Generalized kinetic master plots for the thermal degradation of polymers following a random scission mechanism. *J. Phys. Chem. A.* **2010**, *114*, 7868–7876, doi: 10.1021/jp103171h.
28. Sathiya-Prabhakaran, S.P.; Swaminathan, G.; Viraj, V.J. Thermogravimetric analysis of hazardous waste: Pet-coke, by kinetic models and Artificial neural network modeling. *Fuel* **2021**, *287*, 119470, doi: 10.1016/j.fuel.2020.119470.
29. Vyazovkin, S.; Burnham, A.K.; Criado, J.M.; Pérez-Maqueda, L.A.; Popescu, C.; Sbirrazzuoli, N. ICTAC Kinetics Committee recommendations for performing kinetic computations on thermal analysis data. *Thermochim. Acta* **2011**, *520*, 1–19, doi: 10.1016/j.tca.2011.03.034.
30. Maia, A.A.D.; Cardoso de Morais, L. Kinetic parameters of red pepper waste as biomass to solid biofuel. *Bioresour. Technol.* **2016**, *204*, 157–163, doi: 10.1016/j.biortech.2015.12.055.
31. Kim, Y.S.; Kim, Y.S.; Kim, S.H. Investigation of thermodynamic parameters in the thermal decomposition of plastic waste−waste lube oil compounds. *Environ. Sci. Technol*. **2010**, *44*, 5313–5317, doi:10.1021/es101163e.
32. Anca-Couce A.; Tsekos C.; Retschitzegger, S; Zimbardi, F.; Funke, A; Banks, S.; Kraia, T.; Marques, P.; Scharler, R.; de Jong, W.; Kienzl, N. Biomass pyrolysis TGA assessment with an international round robin. *Fuel* **2020**, *276*, 118002, doi: 10.1016/j.fuel.2020.118002.
33. Kappert, E.J.; Bouwmeester, H.J.M.; Benes, N.E.; Nijmeijer, A. Kinetic analysis of the thermal processing of silica and organosilica. *J. Phys. Chem. B* **2014**, *118*, 5270–5277, doi: 10.1021/jp502344k.
34. Ozawa, T. Kinetics of non-isothermal crystallization. *Polymer* **1971**, *12*, 150–158, doi: 10.1016/0032-3861(71)90041-3.
35. Doyle, C.D. Estimating isothermal life from thermogravimetric data. *J. Appl. Polym. Sci.* **1962**, *6*, 639–642, doi: 10.1002/app.1962.070062406.
36. Muigai, H.H; Choudhury, B.J.; Kalita, P.; Moholkar, V.S. Co-pyrolysis of biomass blends: Characterization, kinetic and thermodynamic analysis. *Biomass Bioenergy* **2020**, *143*, 105839, doi: 10.1016/j.biombioe.2020.105839.
37. Xiao, H.; Jiang, K.; Chen, Y.; Lei, Z.; Chen, K.; Cheng, X.; Qi, J.; Xie, J.; Huang, X.; Jiang, Y. Kinetics and thermodynamic analysis of recent and ancient buried *Phoebe zhennan* wood. *ACS Omega* **2020**, *5*, 20943-20952, doi: 10.1021/acsomega.0c02395.